Cyclotron resonance maser experiments in a bifilar helical waveguide

Alon Aharony, Rami Drori, and Eli Jerby*
Faculty of Engineering, Tel Aviv University, Ramat Aviv 69978, Israel
(Received 24 January 2000)

Oscillator and amplifier cyclotron-resonance-maser (CRM) experiments in a spiral bifilar waveguide are presented in this paper. The slow-wave CRM device employs a low-energy low-current electron beam (2–12 keV, ~0.5 A). The pitch angle of the helical waveguide is relatively small; hence, the phase velocity in this waveguide, $V_{ph} \cong 0.8c$ (where c is the speed of light), is much faster than the axial velocity of the electrons, $V_{ez} \leqslant 0.2c$. Thus traveling-wave-tube-type interactions are eliminated in this device. According to the CRM theory, the dominant effect in this operating regime, $V_{ez} < V_{ph} < c$, is the axial (Weibel) bunching mechanism rather than the opposed azimuthal bunching mechanism. In an oscillator mode, the CRM output frequency is tuned continuously in the range 2.5–8.4 GHz by varying the axial magnetic field. A fine-tuning is possible by the electron accelerating voltage. In the amplifier mode, this CRM experiment demonstrates an amplification up to 16 dB at 5 GHz. The immediate gain bandwidth is wider than 0.1 GHz (>2%). The wide tunable range of this CRM device due to the nondispersive bifilar helix is discussed.

PACS number(s): 52.75.Ms, 84.40.Ik, 84.40.Az

I. INTRODUCTION

Cyclotron resonance masers (CRM's) and related gyrodevices are known as high-power sources of microwaves and millimeter waves. In particular, gyroamplifiers can produce high gain, and therefore they can be useful to boost the output power of a variety of existing microwave systems. Recently, a record of a 70-dB gain in a gyrotraveling-wave amplifier (TWA) experiment was reported by Chu *et al.* [1]. Another recent gyro-TWA experiment, in a novel helical waveguide structure [2], has yielded an output power of 1 MW, a gain of 23 dB, efficiency of 20%, and an instantaneous bandwidth of more than 10%. This helical CRM device operates in the fast-wave regime [$V_{ph} > c$, where V_{ph} is the electromagnetic (em) phase velocity and c is the speed of light]. In another recent CRM amplifier experiment, a gyrotwystron obtained a 50-kW peak output power in the *W* band (94 GHz) [3].

In general, gyroamplifiers seem to be promising in terms of high-amplification levels, high-peak and average powers, and high operating frequency. In all these aspects, gyroamplifiers are superior with respect to conventional (*O*-type) traveling-wave tubes (TWT's) [4,5]. However, gyroamplifiers are limited by their inferior tunability and bandwidth performance. The cyclotron-resonance mechanism dictates, inherently, a narrow bandwidth (much narrower than the multioctave *O*-type TWT). The tunability range of gyrodevices is limited also by the static magnetic field and by the hollow waveguide dispersion.

In this paper, we demonstrate a widely tunable CRM scheme. The device incorporates the CRM interaction within a bifilar helical waveguide, which supports mildly slow waves (note that Ref. [2] describes a fast-wave CRM device). The single-helix waveguide, common in *O*-type TWT's, was proposed also for slow-wave CRM's in 1983 [6], but to our best knowledge it was never reported experimentally. The nondispersive helix [7] enables a CRM operation in a wide tunable range.

The slow-wave propagation in the range $V_{ez} < V_{ph} < c$, where V_{ez} is the electron axial velocity, modifies the CRM operation from the conventional gyrotron mode to the Wiebel interaction [8], i.e., from the azimuthal- to the axial-bunching-dominated CRM interaction. The bifilar helical waveguide in our schemes enhances the transverse-wave components, which are essential for the CRM operation.

Unlike the TWT, which requires a strict reduction of the phase velocity to the speed of the electron beam (i.e., $V_{ph} \cong V_{ez}$), the slow-wave CRM may tolerate a relatively large phase-velocity range just below the speed of light (i.e., $V_{ph} \lesssim c$ and $V_{ph} \gg V_{ez}$). This enables a much wider waveguide aperture and a much more rigid slow-wave structure as compared to the conventional *O*-type TWT with a delicate helix. Consequently, the output power of the slow-wave CRM could be much larger than that of the *O*-type TWT.

In this paper, Sec. II presents the experimental setup of the bifilar-helix CRM in oscillator and amplifier schemes. Section III describes the experimental results in both schemes, and Sec. IV presents our conclusions.

II. EXPERIMENTAL SETUP

The bifilar-helix CRM, illustrated in Fig. 1, consists of two copper strips helicaly wound on a glass tube (outside the vacuum). The experimental device is sketched in Fig. 2. It consists of a planar cathode inside a glass vacuum tube, a bifilar helix around this tube (shown also in Fig. 1), a solenoid, and a kicking anode which imparts transverse velocity to the electrons. The waveguide conductors are wound on the outside surface of the glass vacuum tube for the experimental convenience of modifying the waveguide during the experiment under vacuum conditions.

The electron beam is generated by a dispenser thermionic cathode (Spectra Mat, STD 200). A narrow metallic cylinder tight around outside the glass tube is used as both an anode and a kicker. The electron-beam diameter after kicking is

*FAX:+972-3-6423508. Email address: jerby@eng.tau.ac.il

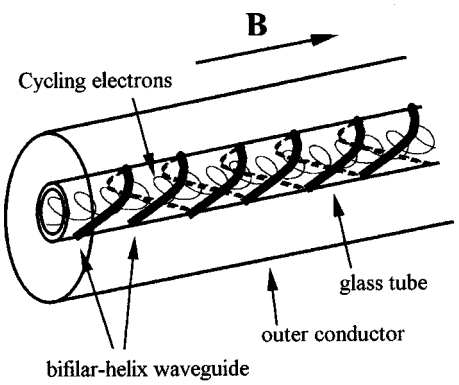

FIG. 1. A schematic of the bifilar helical waveguide used in the CRM experiment.

$\sim$10 mm. A Faraday cup collector at the waveguide end is connected to the ground through a 50-Ω resistor. The voltage drop on this resistor during the pulse measures the electron beam current.

Synchronized pulsers generate the solenoid and the *e*-gun pulses, as described in Ref. [9]. The electron-gun high-voltage pulser and the kicker high-current pulser are triggered at the peak of the solenoid pulse. A dc high-voltage power supply is used to shape the beam optics. The uniform solenoid magnetic field maintains the electron cyclotron motion along its axis. The electron beam is injected inside the glass tube and interacts with the electromagnetic wave supported by the waveguide conductors outside the glass tube. The experimental parameters are listed in Table I.

The experiment is operated in either an amplifier or oscillator mode. In the amplifier scheme, the bifilar waveguide is matched to coaxial cables at the input and output ports. In the oscillator scheme, both ports are shortened, and the rf power is sampled by a small probe. The rf power generated by the cyclotron interaction is detected, attenuated, filtered, and splitted into two arms. In the power measurement arm, the signal is detected using a power detector (HP423b). In the frequency measurement arm (in the oscillator configuration only), the signal frequency is measured using a frequency-time analyzer (HP5372A). The pulsed gun voltage, the collected *e*-beam current, and the solenoid current are measured simultaneously.

Considering the long period of the helical waveguide, a quasi-TEM mode profile is approximated as a solution of the Laplace equation with the appropriate boundary conditions. The transverse profile of the em mode, supported by bifilar striplines, is shown in Figs. 3(a) and 3(b). Cold measurements of the bifilar helical waveguide (in the absence of the electron beam) have been carried out using a vector network analyzer (HP8510C). Reflection measurements of the 38-cm-long oscillator cavity show resonance frequencies (i.e., axial modes) every $\Delta f = 305$ MHz. Another measurement, of the transmission delay time in a 25-cm-long amplifier tube, results in a delay time of 1.07 ns. Both measurements, in frequency and time domains, indicate a phase velocity of V_{ph}

TABLE I. Experimental parameters.

Electron beam		
Energy	1–12	[keV]
Current	0.1–0.8	[A]
Pulse width	$\sim$1	[ms]
Bifilar helix waveguide		
Glass tube diameter	20	[mm]
Helix pitch period	125	[mm]
Strip width	10	[mm]
Waveguide length:		
Amplifier	250	[mm]
Oscillator	380	[mm]
Magnetic field (uniform solenoid)	0.5–3.0	[kG]
Frequency range	2.4–8.5	[GHz]

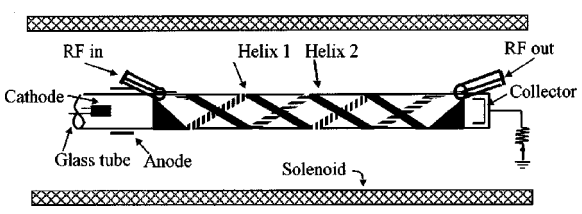

FIG. 2. The CRM experimental device.

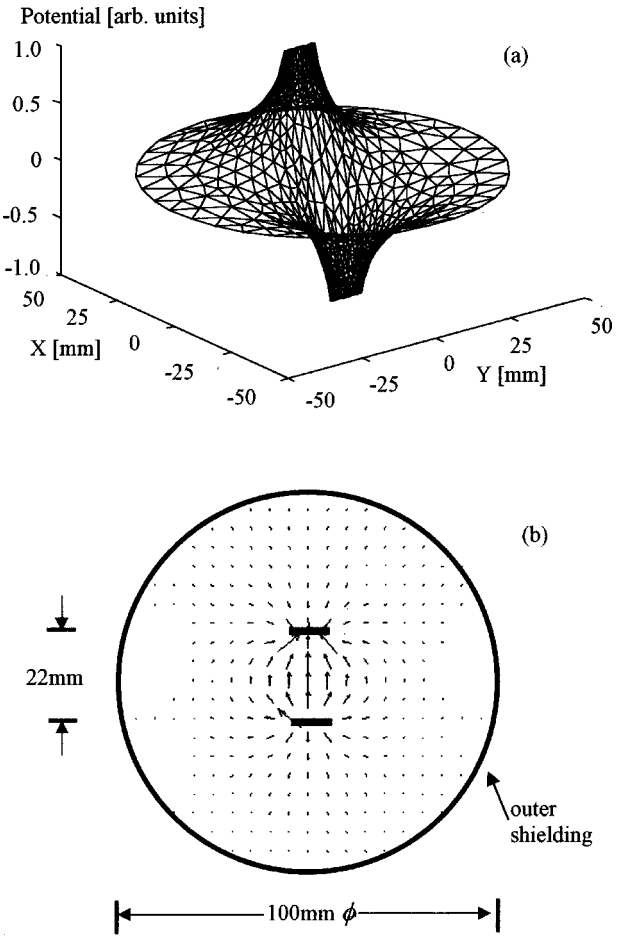

FIG. 3. Transverse profiles of a quasi-TEM mode in a double stripline waveguide. The electric potential (a) and field (b) profiles.

$=0.77c$. In the helical waveguide, this em phase velocity is much faster than the electron axial velocity, $V_{ez}<0.2c$.

III. EXPERIMENTAL RESULTS

The bifilar-helix CRM experiment was studied in both oscillator and amplifier schemes. The experimental results for both schemes are presented in the following sections.

A. Oscillator experiment

The bifilar-helix CRM is operated as an oscillator when both input and output ports of the waveguide are shorten to form of a resonator. A typical run of the oscillator experiment is shown in Figs. 4(a), 4(b), and 4(c). Figure 4(a) shows the electron-gun voltage and the corresponding electron-beam current measured in the collector. The solenoid field in this run is 2.17 kG, which corresponds to a nonrelativistic cyclotron frequency of 6.06 GHz. Figure 4(b) shows the microwave power detector output. Figure 4(c) shows the instantaneous radiation frequency. The latter was measured by a frequency-time analyzer (HP 5372A) with a 7.00-GHz local oscillator. Figure 5 shows the CRM radiation frequency with respect to the electron-gun voltage, as obtained from the results shown in Figs. 4(a) and 4(c). A negative tendency of the CRM oscillation frequency with respect to the electron energy is clearly seen.

The CRM oscillator frequency is tuned by varying the solenoid field. Figure 6 presents data accumulated in 50 experimental runs. Each cross represents a different CRM run. The results show the radiation frequency versus the cyclotron frequency for a 9-kV electron-gun voltage in each run. The dashed line in Fig. 6 shows the linear best fit. The CRM tunability is demonstrated in this experiment over almost two octaves. The wide frequency range of 2.4–8.4 GHz, is bounded in this setup by the electron optics in the low limit and by the maximum available magnetic field in the high limit. Hence even a wider tunability range could be expected in an improved experimental setup.

B. Amplifier experiment

In the CRM amplifier experiment, both ends of the bifilar helical waveguide are matched to coaxial connectors. An rf signal with constant power level is injected into the input port. A typical run of the bifilar-helix CRM amplifier experiment is shown in Figs. 7(a) and 7(b). In this run $B \cong 1.73$ kG and the input rf power is 1 W. The electron-gun voltage and collector current are shown in Fig. 7(a), and the detector output voltage, which indicates the total rf power output, is shown in Fig. 7(b). The reference level due to the constant input power injection is observed before the gun voltage pulse is commenced. Power levels below this reference indicate CRM absorption, whereas higher power levels indicate amplification.

The amplification behavior shows a symmetry in the leading and falling edges of the voltage pulse in a shape of ''rabbit ears.'' During the first amplification period, the electron current is larger than that in the second one; thus, the first amplification peak is higher than the second one. Each gain burst in Fig. 7(b) is accompanied by a CRM absorption ''valley'' which appears in higher voltages than the amplification in both pulses.

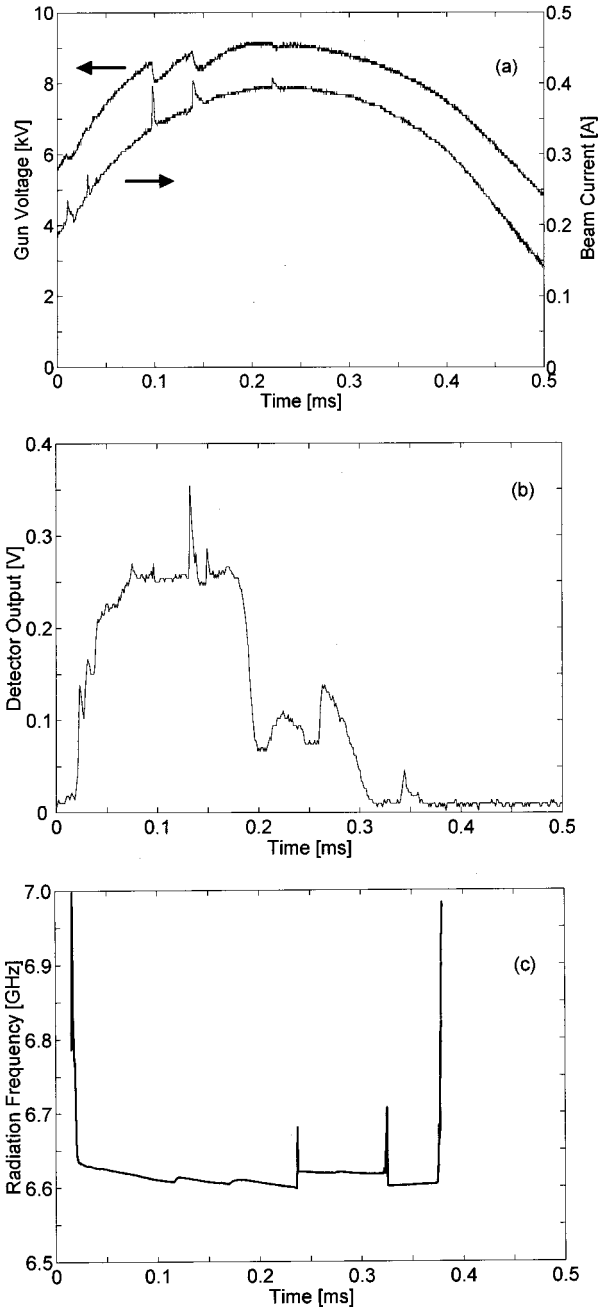

FIG. 4. A typical CRM oscillator run. The electron-gun voltage and beam current (a). The rf detector output (b) and the measured radiation frequency (c).

A net CRM amplification of 16 dB, as shown in Fig. 7(a), is reached for a gun voltage of around 2 kV and a beam current of 0.2 A. This excludes the waveguide losses (~8 dB of insertion and matching losses), which reduces the overall amplification in this experimental setup to 8 dB and the net efficiency to 2%.

The immediate amplification bandwidth near the resonance frequencies is shown in Fig. 8. This graph is obtained for three different *e*-gun voltages (4.38, 4.88, and 5.38 kV) from 16 runs of the slow-wave CRM amplifier experiment at the same magnetic field (1.60 ± 0.08 kG). The immediate

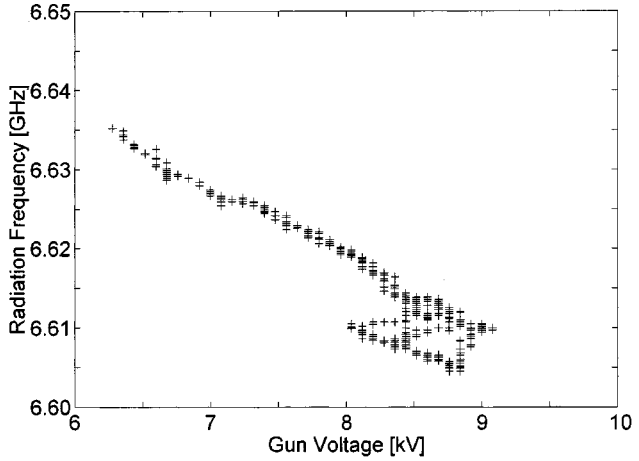

FIG. 5. The CRM radiation frequency dependence on the electron-gun voltage.

frequency bandwidth is found to be larger than 0.1 GHz in each of these three voltages. Figure 8 shows also how the CRM center frequency is tuned by the electron-gun voltage.

IV. DISCUSSION

In the CRM oscillator experiment, the frequency is controlled mainly by the axial magnetic field. The oscillation frequency is slightly higher than the cyclotron frequency; hence, the CRM interaction occurs with a forward wave. Figure 6 shows a closely linear relation between the cyclotron frequency f_c and the radiation frequency f. This experimental relation obeys the linear equation

$$f \cong 1.106 f_c - 25\,\mathrm{MHz}, \tag{1}$$

which indicates a ~10% Doppler shift. Substituting Eq. (1) into the known CRM tuning relation $\omega = \omega_c + k_z V_{ez}$, where ω is the radiation frequency, ω_c is the cyclotron frequency, and $k_z = \omega / V_{\mathrm{ph}}$ is the axial wave number, enables us to evaluate the effective electron axial velocity $V_{ez} = 0.07c$. Consequently, the mean electron velocity pitch ratio is evaluated as $V_\perp / V_{ez} \cong 2.3$.

A fine-tuning of the radiation frequency is performed by slightly varying the electron energy. Figure 5 shows how the radiation frequency declines as the gun voltage increases. The electron axial velocity is relatively small; hence, the Doppler shift varies slowly with the electron energy. The dominant effect here is therefore the variation of the relativistic cyclotron frequency by the electron energy.

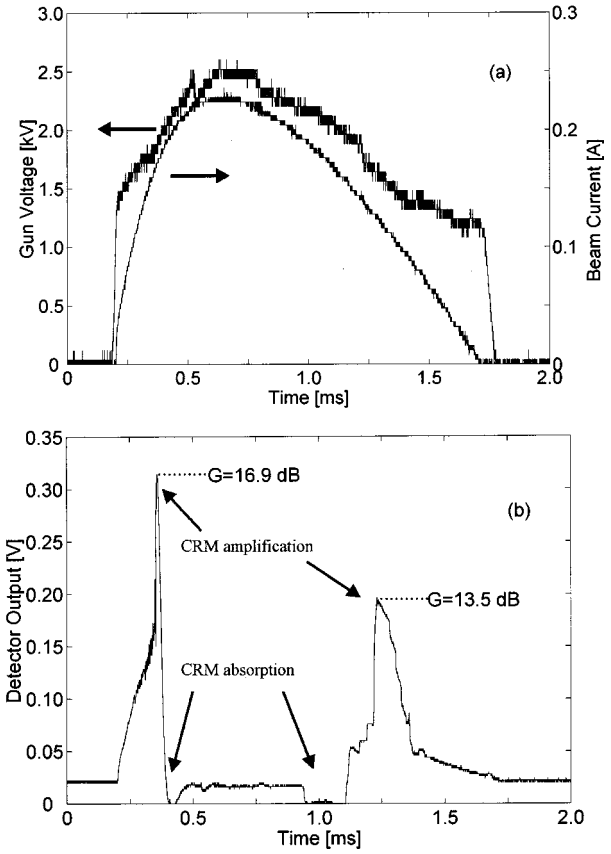

FIG. 7. A typical CRM amplifier run. The electron-gun voltage and beam current (a). The microwave detector output (b).

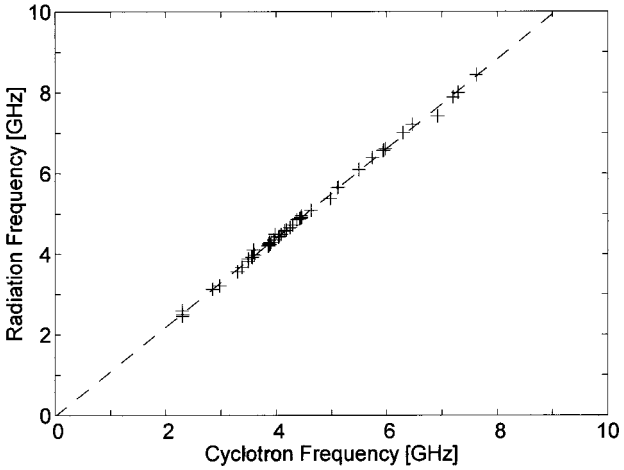

FIG. 6. The CRM tunability. The radiation frequency vs the cyclotron frequency. Measurements are denoted by +'s, and the dashed line shows their best linear fit.

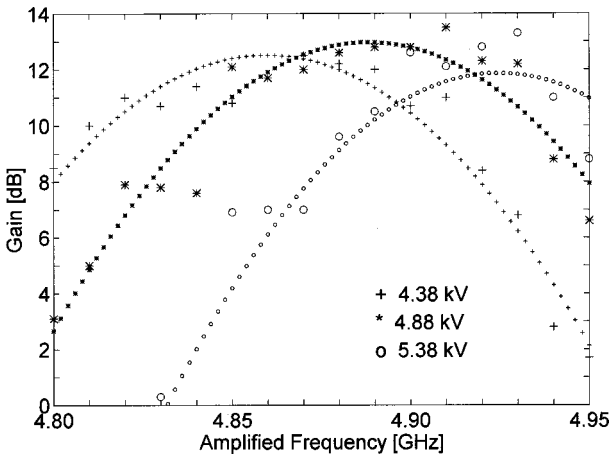

FIG. 8. The CRM amplifier instantaneous bandwidth. The +,*, and ○ denotes measurements in 4.38, 4.88, and 5.38 kV, respectively. The curves show their best parabolic fits.

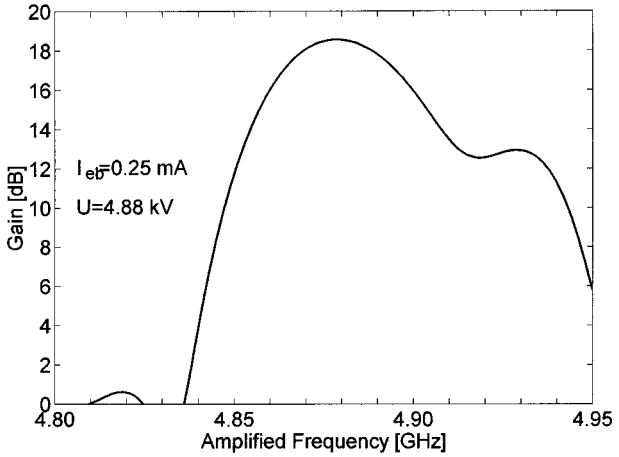

FIG. 9. The calculated gain vs frequency of the CRM amplifier (4.88-kV, 0.25-A electron beam) using the linear model in the Appendix.

A linear analysis of this experiment was conducted using a slow-wave CRM linear model [10] as presented in the Appendix. The experimental measurements and the results of electron-beam optic simulations [11] were verified by this analysis. In particular, for the CRM oscillator parameters, a sufficient gain for oscillations buildup is obtained for a 2.3 pitch ratio with a frequency shift off resonance of around -25 MHz.

The bifilar-helix (slow-wave) CRM device operates as an oscillator and as an amplifier in a wide frequency range. The use of a bifilar helix waveguide with a small pitch angle enables in principle a high-power cyclotron interaction with a wide frequency tuning capability. The CRM interaction was observed over almost two octaves, from 2.4 GHz, continuously, up to 8.4 GHz. A net CRM amplification of 16 dB (peak) was achieved with an instantaneous bandwidth >0.1 GHz of around 5 GHz.

Various directions are being considered for the continuation of this study and for its implementation in practical CRM amplifiers.

APPENDIX: A LINEAR MODEL OF THE SLOW-WAVE CRM

In the linear regime, the cyclotron interaction near resonance is described by a fourth-order Pierce-type dispersion equation. The transfer ratio of the electromagnetic wave along the interaction regime is given by [10] in the Laplace complex plane as follows:

$$\tilde{T}(\hat{s},\omega)=\frac{(\hat{s}-\hat{\theta})^2(\hat{s}+2\hat{\beta})}{\hat{s}(\hat{s}-\hat{\theta})^2(\hat{s}+2\hat{\beta})-(\hat{s}+\hat{\beta})Q_c(\hat{s},\omega)}, \quad \text{(A1)}$$

where the s variable is defined as a complex wave number in accordance with the known Laplace transform $\tilde{T}(s)=\int T(z)e^{-(s+j\beta)z}$, where β is the axial wave number and θ is the interaction tuning parameter. All parameters are normalized to the waveguide length L as

$$\hat{s}=jsL, \quad \text{(A2a)}$$

$$\hat{\beta}=\beta L, \quad \text{(A2b)}$$

$$\hat{\theta}=(\omega-\omega_0-\beta V_{0z})L/V_{0z}, \quad \text{(A3)}$$

where V_{0z} is the initial axial velocity of the electrons. The coupling term between the em wave and the spiraling electron beam is given by

$$Q_c(\hat{s},\omega)=\frac{1}{2}\hat{\theta}_p^2F_f\left((\hat{s}-\hat{\theta})\beta_{ez}(\hat{Z}-\beta_{ez})+\frac{1}{2}\beta_{e\perp}^2(\hat{k}\hat{Z}-\hat{s}-\hat{\beta})\right), \quad \text{(A4)}$$

where $\beta_{ez}=V_{0z}/c$, $\beta_{e\perp}=V_{0\perp}/c$, F_f is the effective filling factor of the electron beam in the interaction cross section, and $\hat{Z}$ is the normalized impedance of the waveguide. The effective normalized electron plasma frequency is $\hat{\theta}_p=\sqrt{e^2n_0/\gamma_0m\varepsilon_0}L/V_{0z}$, where ε_0 is the vacuum dielectric permitivity and n_0 is the electron-beam density. The dispersion equation was solved numerically for a 4.88-kV, 0.25-A electron beam. Figure 9 shows the instantaneous CRM gain bandwidth as results from the linear model. In a comparison with the experiment (Fig. 8), the model shows a higher gain and a narrower width than the experimental instantaneous gain curve. These differences are attributed to the velocity spread in the experiment, which is ignored in the model.

[1] K. R. Chu, H. Y. Chen, C. L. Hung, T. H. Chang, L. R. Barnett, S. H. Chen, T. T. Yang, and D. J. Dialetis, IEEE Trans. Plasma Sci. **27**, 391 (1999).
[2] G. G. Denisov, V. L. Bratmann, A. W. Cross, W. He, A. D. R. Phelps, K. Ronald, S. V. Samsonov, and C. G. Whyte, Phys. Rev. Lett. **81**, 5680 (1998).
[3] M. Blank, B. G. Danly, and B. Levush, IEEE Trans. Plasma Sci. **27**, 405 (1999).
[4] M. Thumm (unpublished).
[5] V. L. Granatstein, R. K. Parker, and C. M. Armstrong, Proc. IEEE **87**, 702 (1999).
[6] H. S. Uhm and J. Y. Choe, Phys. Fluids **26**, 3418 (1983).
[7] J. R. Pierce and P. K. Tien, Proc. IRE **1954**, 1389 (1954).
[8] V. L. Granatstein and I. Alexeff, *High-Power Microwave Sources* (Artech House, Boston, 1987), and references therein.
[9] E. Jerby, A. Shahadi, V. Grinberg, V. Dikhtiar, M. Sheinin, E. Agmon, H. Golombek, V. Trebich, M. Bensal, and G. Bekefi, IEEE J. Quantum Electron. **31**, 970 (1995).
[10] E. Jerby, Phys. Rev. E **49**, 4487 (1994).
[11] W. B. Herrmannsfeldt (unpublished).